Inductive Plasma Thruster (IPT) for an Atmosphere-Breathing Electric Propulsion System: Design and Set in Operation

IEPC-2019-A-488

Presented at the 36th International Electric Propulsion Conference
University of Vienna • Vienna, Austria
September 15-20, 2019

Francesco Romano[1,aa] and Georg Herdrich[2,aa]
[aa] *Institute of Space Systems (IRS), University of Stuttgart, Pfaffenwaldring 29, 70569, Germany*

Peter C.E. Roberts[3,a] A. Boxberger[aa], Y.-A. Chan[aa], C. Traub[aa], S. Fasoulas[aa], K. Smith[a], S. Edmondson[a], S. Haigh[a], N. Crisp[a], V. T. Abrao Oiko[a], R. Lyons[a], S. D. Worrall[a], S. Livadiotti[a], C. Huyton[a], L. Sinpetru[a], R. Outlaw[a], J. Becedas[b], R. M. Dominguez[b], D. González[b], V. Hanessian[c], A. Mølgaard[c], J. Nielsen[c], M. Bisgaard[c], D. Garcia-Almiñana[d], S. Rodriguez-Donaire[d], M. Sureda[d], D. Kataria[e], R. Villain[f], J. Santiago Perez[f], A. Conte[f], B. Belkouchi[f], A. Schwalber[g], B. Heißerer[g], M. Magarotto[h], D. Pavarin[i]

[a] *The University of Manchester, Manchester,* George Begg Building, Sackville Street, Manchester, M13 9PL, UK.
[b] *Elecnor Deimos Satellite Systems,* Calle Francia 9, 13500 Puertollano, Spain
[c] *GomSpace AS,* Langagervej 6, 9220 Aalborg East, Denmark
[d] *UPC-BarcelonaTECH,* Carrer de Colom 11, 08222 Terrassa, Barcelona, Spain
[e] *Mullard Space Science Laboratory (UCL),* Holmbury St. Mary, Dorking, RH5 6NT, United Kingdom
[f] *Euroconsult,* 86 Boulevard de Sébastopol, 75003 Paris, France
[g] *concentris research management gmbh,* Ludwigstraße 4, D-82256 Fürstenfeldbruck, Germany
[h] *Center of Studies and Activities for Space "Giuseppe Colombo" - CISAS,* Via Venezia 15, 3513 Padua, Italy
[i] *Università degli Studi di Padova, Industrial Engineering Department DII,* Via Gradenigo 6/a, 3513 Padua, Italy

Abstract: Challenging space missions include those at very low orbits, where the atmosphere is source of significant drag on a satellite. Therefore, an efficient drag-compensation propulsion system is required to extend the mission lifetime. One solution is Atmosphere-Breathing Electric Propulsion (ABEP), a system that collects atmospheric particles and directly uses them as propellant for an electric thruster, therefore minimizing the requirement of limited propellant availability. The system is theoretically applicable to any celestial body with atmosphere. This would enable new mission types due to the new altitude ranges available for continuous orbiting. Challenging is also the presence of reactive chemical species, such as atomic oxygen in Earth orbit, erosion source of (not only) the propulsion system components, i.e. acceleration grids, electrodes and discharge channels of conventional EP systems such as RIT and HET. IRS is developing within the DISCOVERER project an intake and a thruster for an ABEP system. This paper, deals with the design of novel contact-less RF thruster, the inductive plasma thruster (IPT) based on a novel antenna design.

[1] Research Associate, Institute of Space Systems (IRS), romano@irs.uni-stuttgart.de
[2] Head Plasma Wind Tunnels and Electric Propulsion, Institute of Space Systems (IRS), herdrich@irs.uni-stuttgart.de
[3] Lecturer, School of Mechanical, Aerospace and Civil Engineering, peter.c.e.roberts@manchester.ac.uk

Nomenclature

ABEP	=	atmosphere-breathing electric propulsion
EM	=	electromagnetic
EP	=	electric propulsion
IPG	=	inductively heated plasma generator
IPT	=	inductive plasma thruster
MRI	=	magnetic resonance imaging
RF	=	radio frequency
VLEO	=	very-low Earth orbit

I.Introduction

THE Inductive Plasma Thruster IPT at IRS is designed with the EU H2020 DISCOVERER project, that aims to redesign very low Earth orbit (VLEO <400 km) platforms by investigating low drag materials, aerodynamic attitude control, and by developing an Atmosphere-Breathing Electric Propulsion system (ABEP) see Figure 1. Orbiting at very low altitudes around Earth can open a new range of opportunities for space missions, however, mission's lifetime is very limited due to aerodynamic drag. Therefore, to obtain longer mission lifetimes, the spacecraft requires a propulsion system that efficiently compensates the drag. One solution, is employing an ABEP system. Such systems collects the atmospheric particles at VLEO by means of an intake, and uses them as propellant by feeding an electric thruster, which ionizes and accelerates them for thrust generation. Such system removes the lifetime limit due to the available propellant on-board, by using the residual atmospheric gas that causes the drag, as the source for the thrust. Such propulsion system has to cope with N_2 and O as propellant. The approach within DISCOVERER is of an RF-based contact-less thruster, so to remove any issue of performance degradation over time due to operation with atomic oxygen O as propellant.

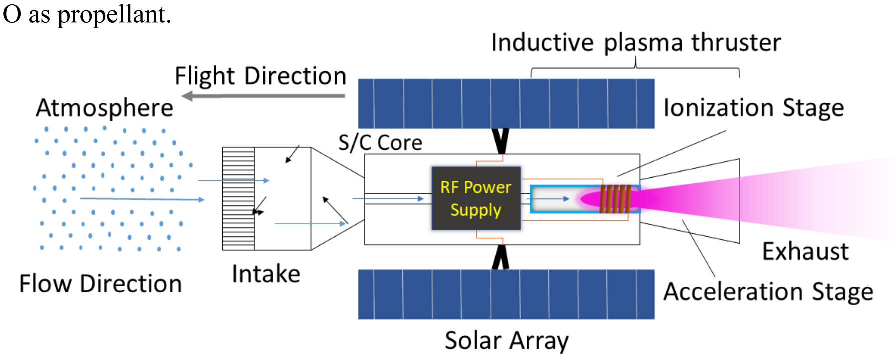

Figure 1. ABEP Concept [1]**.**

II. Inductive Plasma Thruster

The procedure of the IPT design is described in the following sections.

A. IPT Design Approach

The starting point of the IPT has been the long-term heritage at IRS of inductive plasma generators (IPG). Refurbishment and upgrades have been performed on the small scaled inductively heated plasma generator IPG6-S and its facility in the last years [1], [2]. Recent test campaigns have shown the increase of power absorption by applying an external magnetic field to the plasma source [3] and hence approved the feasibility of an advanced IPT that makes use of applied fields to trigger wave mode excitation and, possibly, to operate as EM-based acceleration system. The requirements within the DISCOVERER project are of an RF plasma thruster capable to operate with N_2 and O as propellant at an input power < 5 kW. The device, especially due to the aggressive nature of atomic oxygen that is one of the most prominent species in VLEO, has to avoid any direct contact with the plasma to reduce any erosion phenomena to a minimum, as this will reduce thruster's performance over mission's lifetime [4], [5]. Moreover, a plasma plume that is already neutral is a great advantage due to the difficulty of realising a neutralizer operating on atmospheric propellant [6], [7]. The first version of the IPT is a laboratory device with maximum (technical) flexibility and passive cooling to allow easy modifications for the required optimization. After the design of mechanical and vacuum interfaces [8], the crucial element of the IPT design is the antenna.

B. IPT Antenna Development

The first approach has been a coil antenna, as the simulations have shown to provide better performance compared to a half-helical antenna, commonly used e.g. for helicon plasma sources [3]. In the first design iteration the focus was a discharge channel of 37 mm inner diameter (due to IPG6-S heritage), and a variable number of turns coil antenna. Various coil antenna configuration, with different number of turns and discharge channel radii have been simulated by using both numerical tools HELIC [9], [10], and ADAMANT [11]. By modelling an RF-based plasma source as a transformer, the plasma is seen as resistance in the circuit. According to Chen [12], this plasma resistance R_P has to be as high as possible, at least greater than the circuit resistance R_c in order to maximize power absorption. The preliminary numerical results [3] lead to a chosen frequency higher than 27.12 MHz, as this leads to easier ignition and better power absorption at higher plasma densities. Finally, a 4kW, 40.68 MHz power supply from Advanced Energy with an auto-matching network was acquired as laboratory model PPU.

The antenna and the plasma have to be modelled as an impedance *Z*, with both real and imaginary components. In particular, the imaginary part of the impedance, the reactance *X*, is directly proportional to the applied frequency and has to be as small as possible to avoid and/or minimize power reflection which then would represent a power loss and hence an efficiency decrease for the thruster. The acquired power supply at f=40.68 MHz introduces an "a priori" higher reactance to the RF circuit. ADAMANT gives as output the impedance *Z*, of the antenna plus the plasma, see Eq. (*1*).

$$\vec{Z} = \vec{R} + j\vec{X}$$
$$X = X_L + X_C = 2\pi f L + \left(-\frac{1}{2\pi f C}\right) \tag{1}$$

The results for different plasma densities, magnetic fields, and antenna geometries lead always to a very high *X* component. Moreover, not only the antenna is to be considered for the IPT circuit design, but the system at the whole, including RF generator, matching network, connectors, and transmission lines [13]. In an RF circuit all the power is transferred from the source (RF generator) to the load (antenna and plasma), only if the load's impedance Z_L matches that of the source Z_S. Industrial standards set RF generators as a 50 Ω load purely resistive source. A matching network is introduced in the IPT circuit to dynamically match the load impedance to the purely resistive Z_S by a system of variable capacitors. While this works as protection for the RF generator, it does not improve the load side. Therefore, an optimum design of the whole RF circuit is required to maximize power transfer from source to load. The plasma is a variable load that implies the need of a dynamic tuning control. An accurate selection of the cabling and connectors between RF generator and matching network, and matching network to IPT has been performed, the relevant schematics are shown in Figure 2.

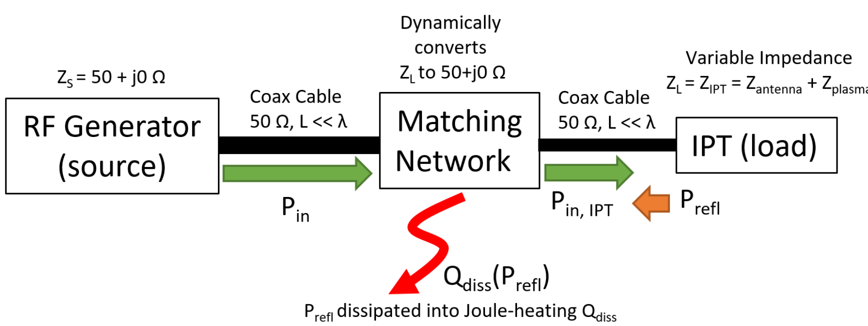

Figure 2 Simplified IPT RF circuit

C. The birdcage antenna

The RF circuit optimization finally lead to the birdcage antenna, a device developed in Magnetic Resonance Imaging (MRI) [14] that provides the required homogeneous magnetic field for such an application. A birdcage antenna operates on the principle that a sinusoidal current distribution on a cylindrical surface will induce a homogeneous transversal magnetic field within the cylindrical volume itself. If operated at a particular resonant mode, this magnetic field is homogeneous. Birdcage antennas are composed by two end-rings, connected by equally spaced rungs (or legs). The rungs and/or the end-rings have capacitors in between to adjust the resonance frequency to the required one. The birdcage antenna can be designed as low-pass, high-pass, or band-pass frequency response. The low-pass has capacitors on the rungs, the high-pass has the capacitors at the end-rings, and the band-pass has capacitors at both locations, see Figure *3*.

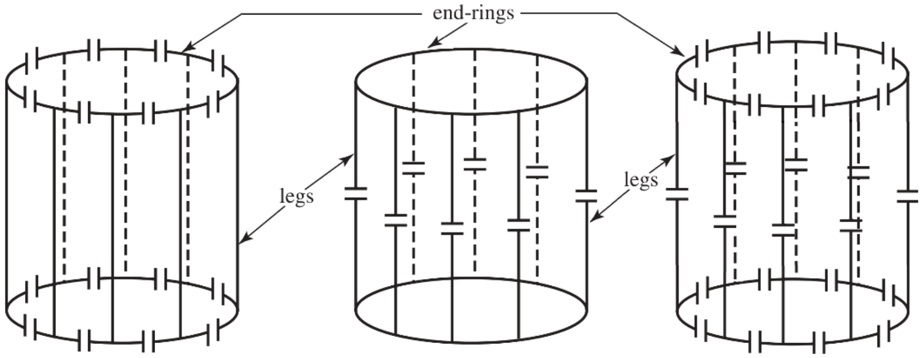

Figure 3 Birdcage Antenna as high-pass (left), low-pass (middle), band-pass (right) (adapted from [15]**).**

Birdcage antennas operate at one of their resonance frequency modes. At such condition, the reactance *X* is zero and its impedance *Z* is purely real, leading to a partially matched load, reducing the requirements for the matching network. Moreover, at the correct resonance, the EM fields are in a promising configuration for a plasma thruster application. Currently, at EPFL helicon plasma is generated for fusion research by birdcage antennas operating at 13.56 MHz for RF powers up to 10 kW [16]–[18]. Moreover, an older study from Guittienne directly investigated the use of birdcage antennas for an helicon based thruster [19].

Each antenna has $k=N/2$ resonant modes. The current distribution along the antenna follows the law described in Eq. (*2*), where I_{jk} is the normalized current at the *j*-th loop for the *k* mode of a birdcage antenna with *N* rungs.

$$I_{jk} = \begin{cases} cos\left(\frac{2\pi jk}{N}\right), & k = 0,1,2,\dots,N/2 \\ \sin\left(\frac{2\pi jk}{N}\right), & k = 1,2,\dots,\left(\frac{N}{2}-1\right) \end{cases} \tag{2}$$

This means that the more rungs there are, the more the current distribution profile along the circumference of the cylinder will match a sinusoidal curve, see Figure 4 (left).

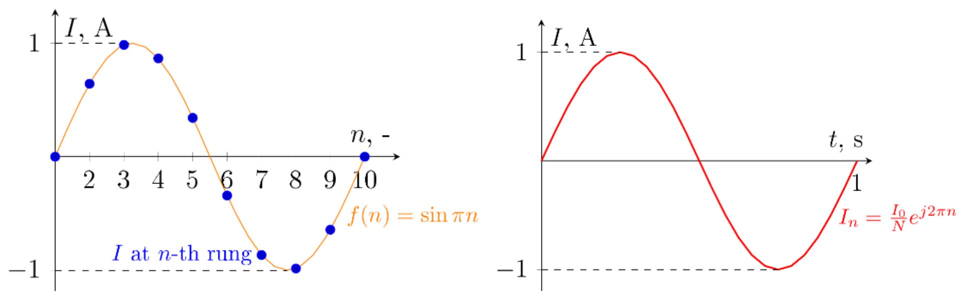

Figure 4 (left) Current distribution along a 10-leg birdcage at a fixed instant of time, (right) current amplitude over time on a single birdcage rung (leg).

Birdcage antennas are modeled by self and mutual inductances of rungs and end-rings, plus the applied capacitances. The resonant frequencies for a low-pass design, are defined as in Eq. (*3*), while for a high pass are given by Eq. (*4*). The high pass design has one resonance mode more (k = 0) at the highest frequency called the AR given by the interaction between the end-rings.

$$\omega_{k_{LP}} = \left[C\left(L_{ER} + 0.5\, L_{Leg} \sin^2 \frac{\pi k}{N}\right)\right]^{-1/2}, \qquad (k = 0,1,2,\dots,N/2) \tag{3}$$

$$\omega_{k_{HP}} = \left[C\left(L_{ER} + 2\, L_{Leg} \sin^2 \frac{\pi k}{N}\right)\right]^{-1/2}, \qquad (k = 0,1,2,\dots,N/2) \tag{4}$$

Here, C is the capacitance of the capacitor for a single gap, L_{ER} and L_{Leg} are the inductances of the end ring and the rung, respectively. Only one resonant mode presents the homogenous magnetic field, for k = 1 at the highest frequency (before the AR) for the high pass configuration, and at the lowest resonating mode for the low pass configuration.

In terms of EM fields, the magnetic field produced by the birdcage is $\vec{B}_1$ considered along y, and the accompanying electric field $\vec{E}_1$ always perpendicular to $\vec{B}_1$, along x. The schematics is shown within Figure *5*. Since $\vec{B}_1$ is linearly polarized, it will switch direction along y on each cycle, and so will $\vec{E}_1$ along x. If the birdcage is fed in quadrature for circular polarization, $\vec{E}_1$ will rotate with $\vec{B}_1$ maintaining the 90° angle between them. An additional external magnetic field provided along the z axis $\vec{B}_0$ is inserted as the one given by the electromagnet.

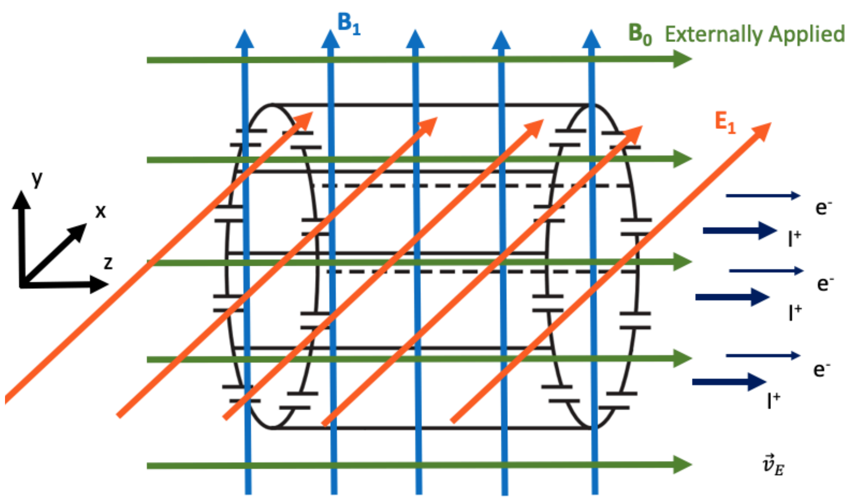

Figure 5 Birdcage EM fields B₁, E₁, externally applied magnetic field B₀.

The combination of these fields, which still excludes the EM fields from the plasma, hints to a drift velocity given by $\vec{v}_E = \vec{E} \times \vec{B}$. Such velocity is the exhaust velocity, and it is imparted to both ions and electrons at the same time and towards the same direction, along z. The thrust, therefore, is provided by both ions and electrons with such velocity, leading to a quasi-neutral plasma exhaust that does not need a neutralizer, see Eq. (*5*). This supports, again, the use of birdcage antenna, with linearly or circularly polarized EM fields, for a plasma thruster application, especially for a neutralizer-free application.

$$\vec{v}_E = \frac{1}{\vec{B}^2} \begin{Vmatrix} \hat{x} & \hat{y} & \hat{z} \\ E_1 & 0 & 0 \\ 0 & B_1 & B_0 \end{Vmatrix} = \frac{1}{{B_0}^2 + {B_1}^2} \begin{Bmatrix} 0 \\ -E_1 B_0 \\ E_1 B_1 \end{Bmatrix} \tag{5}$$

D. IPT Design with a birdcage antenna

The IPT is composed by the propellant injector, the discharge channel, the antenna, the shield, the support structure, and the electromagnet, see Figure 6. The injector is movable along the symmetry axis *z*, by which one can change the discharge channel's length. The external electromagnet is movable along the axis *z* as well, and can produce a magnetic field up to 70 mT at the centre of the discharge channel at a maximum current of 15 A. At such a current more than 30 min operation are possible without overheating, allowing plasma diagnostic measurements to be performed.

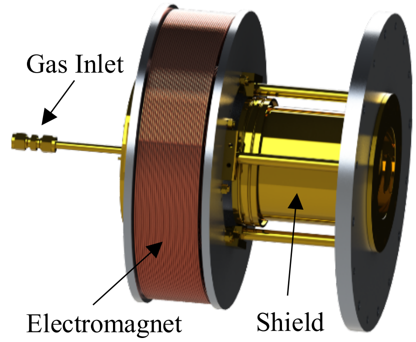

Figure 6 IPT rendering with external electromagnet.

A birdcage with 8 legs in a high pass design has been chosen, designed to resonate at 40.68 MHz with one feeding point, providing a linearly polarized magnetic field. The antenna design requires simulation tools for the resonance tuning and impedance estimation. The commercial 3D EM simulation software Remcom Inc. XFdtd® 7.8.1.3 is used. The birdcage design has to be compatible with the expected currents and voltages for a maximum power of 1.5 kW to allow passive cooling, and to fit the current geometrical requirements. The IPT structure is made of brass to minimize Eddie currents due to the RF fields, and to minimize interactions with the magnetic field fields. The birdcage antenna is enclosed within a brass RF shield that has two main functions: first to isolate the outer environment from the EM fields created by the antenna, and second to isolate the birdcage from external influences. For the resonance study, the full IPT geometry is loaded into the simulation tool. The overall dimensions have been such to allow the mounting on standard ISO-K flanges to minimize the amount of in-house required parts and enabling testing on other standard-based facilities. XFdtd is used to evaluate the resonance frequencies by changing the capacitance value for the whole IPT. Frequency sweeps are performed focusing on the impedance *Z* and the scattering parameter S_{11} over frequency. The S_{11} parameter is generally defined, for a two port system, as the input port voltage reflection coefficient, representing how much power is absorbed and reflected by a load in relation to the input power from a given source.

An example of the resonance study is shown, for the S_{11} parameter in Figure 7 and for the impedance in Figure 8 as the output from XFdtd. Each peak is a resonant frequency and, to verify this, the impedance *Z* is plotted over the frequency as well as in Figure 8. The points at which the reactance *X* passes through the *x*-axis are the resonance frequencies. As expected, for a high-pass 8-leg birdcage, there are *N*/2=4 resonant frequencies plus the anti-resonating AR at the highest frequency. For a high pass, *k=1* is the correct resonance for the homogeneous field.

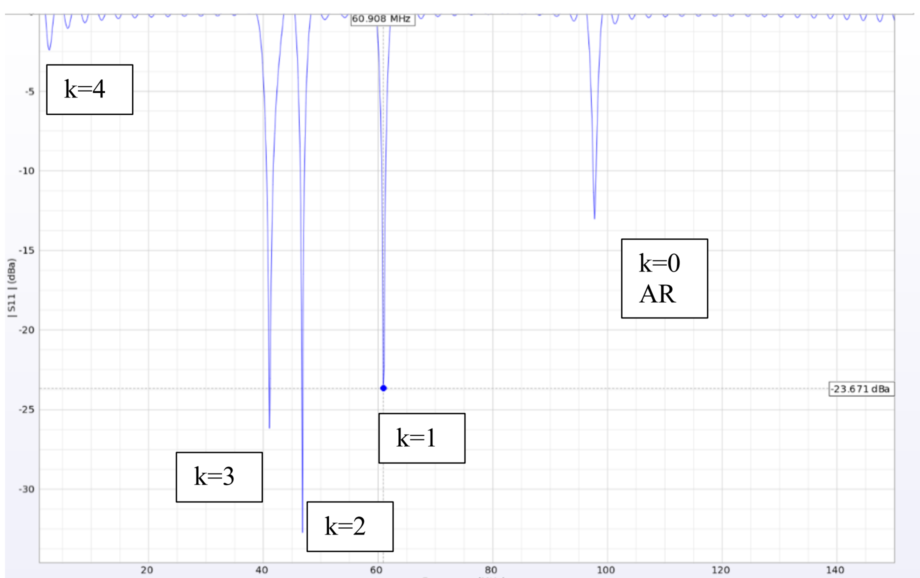

Figure 7 Example of S11 vs f study for a birdcage antenna.

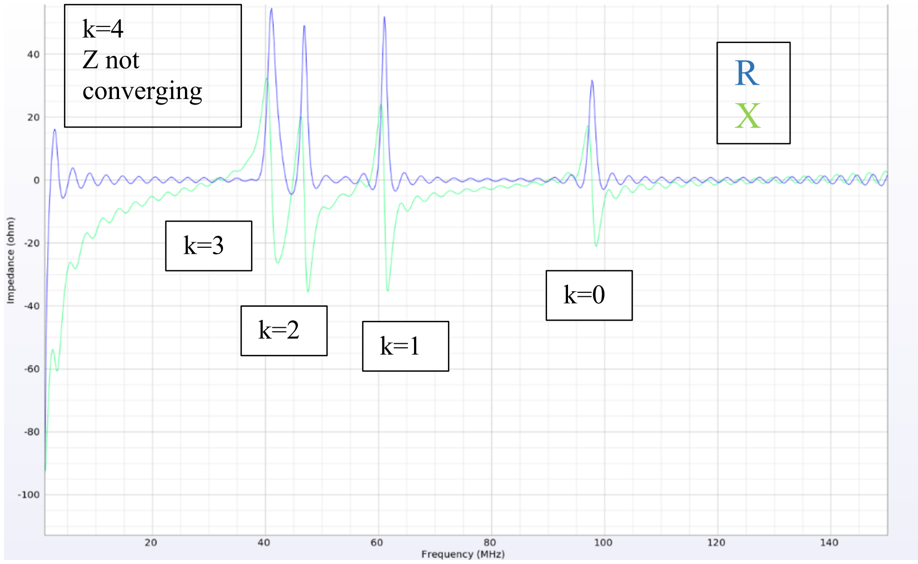

Figure 8 Example of Z vs f study for a birdcage antenna.

For further verification of the resonance frequency to be the correct one, the 3D visualization of transversal electric and magnetic fields is extracted, and compared to that of the other peaks. An example of the correct resonance with a linearly polarized field is shown in Figure 9 for the magnetic field and in Figure 10 for the electric field. At each RF cycle the EM fields reverse their direction.

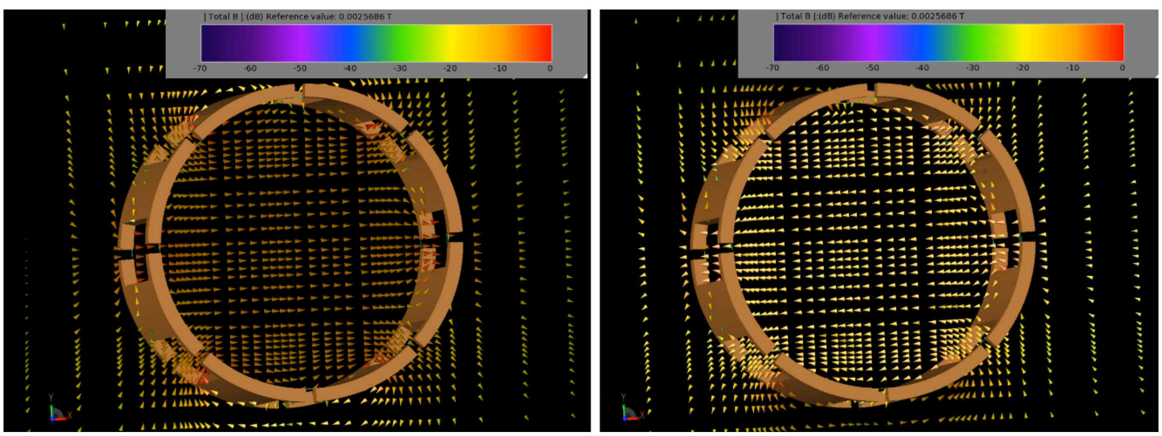

Figure 9 Example of linearly polarized magnetic field of a birdcage antenna at k=1 resonance.

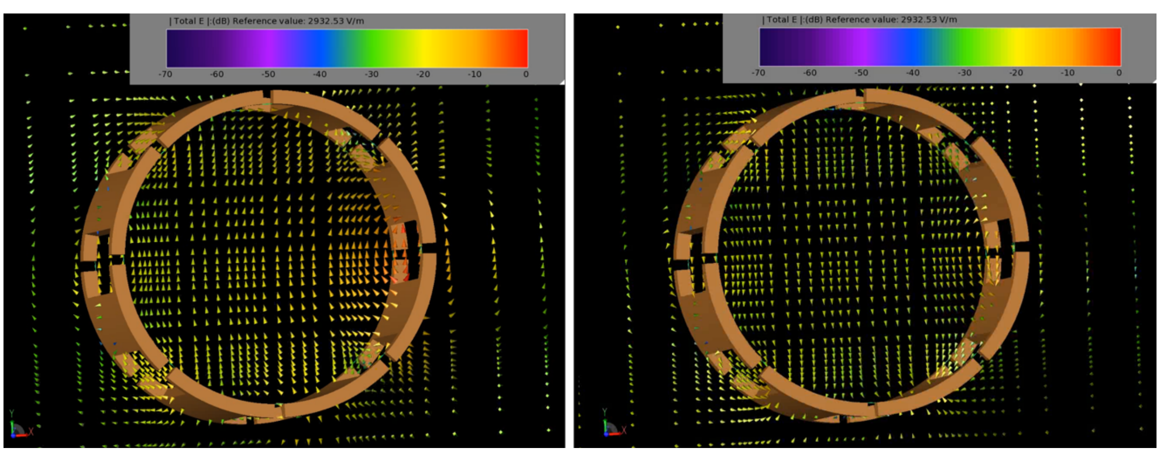

Figure 10 Example of linearly polarized electric field of a birdcage antenna at k=1 resonance.

Once the correct resonance mode is verified, the capacitance value is swept until the peak matches the frequency of 40.68 MHz. The externally applied magnetic field applied by the electromagnet, is expected to aid the formation of helicon waves within the discharge channel therefore providing a high degree of ionization [12], [20].

E. Resonance Tuning

The design for resonance ensures such condition is maintained without plasma. Once the plasma is ignited, however, an impedance change is introduced into the system with both real and imaginary parts. This will produce a resonance frequency shift. Such frequency shift requires tuning, to be shifted back to the original resonant condition. Such issue is already encountered and solved in MRI devices, due to the shift produced by the introduction of bodies within the birdcage antenna [21], [22]. The tuning can be realized, for example, by moving conducting plates that slightly change the circuit properties, in particular X_C and X_L, therefore the resonance frequency. Such tuning is implemented in the IPT by the moving injector, and/or by changing the position and strength of the magnetic field. Such characteristics will be investigated in the coming year. The assembled IPT is shown in Figure 11. Due to a sum of delays, the last missing components of the IPT have arrived just after this conference. After the resonance verification, the ignition is expected before the end of 2019.

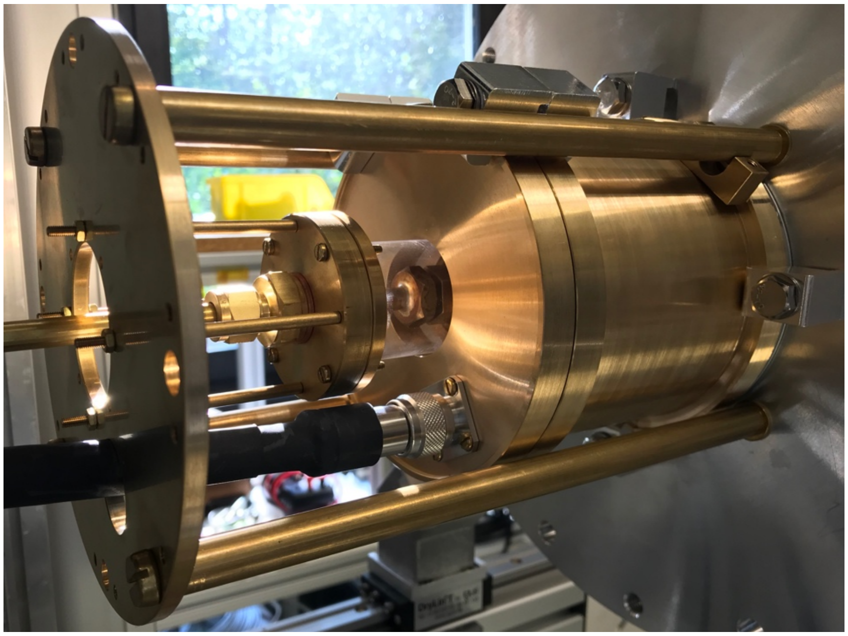

Figure 11 IPT assembled, September 2019

III.Conclusion

An IPT based on a birdcage antenna has been completely designed. Such device takes advantages of a reactance-less configuration with a EM field configuration allowing for a drift for both ions and electrons towards the same direction suggesting a neutral plasma beam leaving the discharge, therefore there is no need of a neutralizer. A RF shield isolates the antenna from the outer environment, and the outer environment from the RF fields. For the future development, such design also provides isolation of spacecraft electronics from the thruster's EM fields. A movable conducting injector can be used to tune the resonance frequency of the IPT, as well as a variable magnetic field, to cope with the frequency shift caused by the plasma. Further work will be the final antenna assembly, the verification of the resonance frequency by means of a network analyser and the first ignition by the end of 2019. First step will be the discharge characterization for different propellant flows, power levels, and magnetic field strengths. Later on, plasma diagnostic will be performed with electrostatic probes, Langmuir and Faraday probes at first, Retarding Potential Analyser and optical emission spectroscopy as next. Further optimization of the magnetic field is on going as starting point for the optimization of plasma acceleration.

Acknowledgments

The DISCOVERER project has received funding from the European Union's Horizon 2020 research and innovation programme under grant agreement No. 737183. This reflects only the author's view and the European Commission is not responsible for any use that may be made of the information it contains. www.discoverer.space

References

[1] F. Romano, B. Massuti-Ballester, T. Binder, G. Herdrich, S. Fasoulas, and T. Schönherr, "System analysis and test-bed for an atmosphere-breathing electric propulsion system using an inductive plasma thruster," *Acta Astronaut.*, vol. 147, no. October, pp. 114–126, 2018.

[2] F. Romano, G. Herdrich, S. Fasoulas, and T. Schönherr, "Performance Evaluation of a Novel Inductive Atmosphere-Breathing EP System," *35th Int. Electr. Propuls. Conf. Atlanta, USA*, vol. IEPC-2017, no. 184, 2017.

[3] S. Masillo *et al.*, "Analysis of electrodeless plasma source enhancement by an externally applied magnetic field for an inductive plasma thruster (IPT).," pp. 3–4.

[4] M. Andrenucci, D. Feili, G. Cifali, D. Valentian, T. Misuri, and P. Rossetti, "Preliminary characterization test of HET and RIT with Nitrogen and Oxygen," no. August, pp. 1–16, 2012.

[5] G. Cifali *et al.*, "Completion of HET and RIT characterization with atmospheric propellants," in *Space Propulsion 2012 2355386*, Bordeaux, 2012.

[6] T. Andreussi *et al.*, "Development and Experimental Validation of a Hall Effect Thruster RAM-EP Concept," in *35th International Electric Propulsion Conference*, Atlanta, USA.

[7] T. Andreussi *et al.*, "Development Status and Way Forward of SITAEL ' s Air-breathing Electric Propulsion," no. August, pp. 1–22, 2019.

[8] F. Romano, G. Herdrich, P.C.E. Roberts, and et al., "Advances on the Inductive Plasma Thruster Design for an Atmosphere-Breathing EP System," *69th Int. Astronaut. Congr. Adelaide, Aust.*, no. IAC-18.C4.6.4x46387, 2018.

[9] F. F. Chen and D. Arnush, "Generalized theory of helicon waves. I. Normal modes," *Phys. Plasmas*, vol. 4, no. 9, pp. 3411–3421, 1997.

[10] D. Arnush and F. F. Chen, "Generalized theory of helicon waves. II. Excitation and absorption," *Phys. Plasmas*, vol. 5, no. 5, pp. 1239–1254, 1998.

[11] D. Melazzi and V. Lancellotti, "ADAMANT: A surface and volume integral-equation solver for the analysis and design of helicon plasma sources," *Comput. Phys. Commun.*, vol. 185, no. 7, pp. 1914–1925, 2014.

[12] F. F. Chen, "Permanent Magnet Helicon Source for Ion Propulsion," *IEEE Trans. Plasma Sci.*, vol. 36, no. 5, pp. 2095–2110, 2008.

[13] A. W. Kieckhafer and M. L. R. Walker, "Rf power system for thrust measurements of a helicon plasma source," *Rev. Sci. Instrum.*, vol. 81, no. 7, pp. 1–8, 2010.

[14] C. E. Hayes, W. A. Edelstein, J. F. Schenck, O. M. Mueller, and M. Eash, "An efficient, highly homogeneous radiofrequency coil for whole-body NMR imaging at 1.5 T," *J. Magn. Reson.*, vol. 63, no. 3, pp. 622–628, 1985.

[15] J. Jin, "Electromagnetics in Magnetic Resonance Imaging - IEEE Antennas and Propagation Magazine," *Clin. Imaging*, vol. 40, no. 6, pp. 7–22, 1998.

[16] A. A. Howling, P. Guittienne, C. Hollenstein, and I. Furno, "Resonant rf network antennas for inductively-coupled plasma sources."

[17] I. Furno *et al.*, "A novel helicon plasma source for negative ion beams for fusion," *Nibs*, no. September, 2016.

[18] I. Furno *et al.*, "Helicon wave-generated plasmas for negative ion beams for fusion," *EPJ Web Conf.*, vol. 157, p. 03014, 2017.

[19] P. Guittienne, E. Chevalier, and C. Hollenstein, "Towards an optimal antenna for helicon waves excitation," *J. Appl. Phys.*, vol. 98, no. 8, 2005.

[20] "First B-dot measurements in the RAID device, an alternative negative ion source for DEMO neutral beams," *Fusion Eng. Des.*, vol. 146, pp. 1140–1144, Sep. 2019.

[21] C. E. Hayes, "The development of the birdcage resonator: A historical perspective," *NMR Biomed.*, vol. 22, no. 9, pp. 908–918, 2009.

[22] A. C. Özen, *Novel MRI Technologies for Structural and Functional Imaging of Tissues with Ultra-short T_2 Values*, vol. 34. KIT Scientific Publishing, 2017.